13th International Symposium on Turbulence and Shear Flow Phenomena (TSFP13)
Montreal, Canada, June 25–28, 2024

ENHANCED RANS MODELING OF SEPARATION INDUCED TRANSITION FLOWS USING FIELD INVERSION

Karim Ahmed, Dylan Sitarski, Anupam Sharma, Paul Durbin
Department of Aerospace Engineering
Iowa State University
Ames, Iowa USA 50011
kahmed@iastate.edu

ABSTRACT

A method for optimizing the prediction of turbulence closure models was introduced by Parish & Duraisamy (2016). The overall method is called FI-ML and it has three main steps. First, a turbulence model is augmented with a corrective field. Then, an optimization problem is solved to find the corrections required to minimize the discrepancies between the turbulence model and high fidelity data (field inversion). Finally, the corrective field is trained against flow features (machine learning). This method has been applied extensively to turbulent flows, and with less extent, to bybass and natural transition. However, field inversion of separation induced transition still needs to be explored. Here, we carry out field inversion for two test cases involving separation induced transition. The first case is a flat plate with favorable and adverse pressure gradients. The second case is a parametric series of NACA 0012 airfoil at four different angles of attack. We explore field inversion with and without a transition model. Both methods show good fitting with the high-fidelity data.

INTRODUCTION

The highly nonlinear behavior of dynamic stall associated with unsteady flow over airfoils usually requires computational investigations (Sharma & Visbal (2019)). Dynamic stall is the delay of the maximum lift beyond its value in static flow. This delay is attributed to the change of effective camber due to the pitching motion and the acceleration of the boundary layer (Magnus effect). Dynamic stall is characterized by the formation and bursting of laminar separation bubbles (LSB) and the formation of a dynamic stall vortex (DSV)— which both play a crucial role in the onset of dynamic stall and in the large overshoots of aerodynamic forces and moments (Sharma & Visbal, 2019). Reynolds averaged Navier-Stokes (RANS) computations have been used to investigate dynamic stall (Visbal, 1990), while large eddy simulations have been deployed more recently for flat plates (Garmann & Visbal, 2011) and airfoils (Visbal & Garmann, 2018). The computationally cost-effective RANS models are known to suffer from inaccuracies in predicting non-equilibrium and separated flows. In addition, flow transition within the laminar separation bubble requires transition models which add more uncertainities. Hence, improving the predictive capability of RANS models for both turbulent and transition flows is needed to effectively investigate dynamic stall.

Transition of laminar-to-turbulent flow occurs through various mechanisms: Natural transition takes place through instabilities in the laminar flow known as Tollmien-Tchlichting waves, when the free-stream turbulence intensity is lower than 1%. For higher turbulence, intensities ($> 1\%$), turbulence penetrates into the laminar boundary layer and disturbances (Klebanoff modes) are generated which grow in amplitude, forcing the flow to transition into turbulence without linear instability of the base state. For flows with adverse pressure gradients, the laminar flow may separate and transition takes place within the separated layer due to the inflection point instability, resulting in the formation of a laminar separation bubble—as discussed previously. These different mechanisms make it difficult for the available transition models to accurately predict aspects such as transition onset, transition length, separation, and reattachment.

Data driven techniques have recently been used to improve the performance of existing RANS models, through data assimilation. One of the earliest implementations of data-driven modeling was quantifying the spatial model-form uncertainties (Oliver & Moser, 2011). The techniques evolved over time to use machine learning models to train model inaccuracies against flow features (Tracey *et al.*, 2013; Wang *et al.*, 2017; Wu *et al.*, 2018; Weatheritt & Sandberg, 2016; Ling *et al.*, 2016). Parish & Duraisamy (2016) introduced the framework of field inversion and machine learning (FIML). The method is to replace a coefficient in the RANS turbulence model by a field $\beta(\mathbf{x})$. Then, an optimization problem is solved to find $\beta(\mathbf{x})$. This has been called a 'model in the loop' approach to data-driven turbulence modeling. It requires that the RANS equations be solved repeatedly, to predict a quantity of interest, as β evolves to optimize the prediction of that quantity. Unlike the aforementioned studies, that rely on learning the functional form of the model from data directly, FIML trains the model in its predictive context. Hence, the trained model is consistent with the CFD implementation. Another virtue of FIML is that the data set can be small or large; a few values of skin friction, or a whole flow field, for example.

FIML has been applied extensively to enhance RANS models for adverse pressure gradients turbulent flows and separated turbulent flows (Duraisamy *et al.*, 2017; Singh *et al.*, 2017; Rumsey *et al.*, 2022; Srivastava *et al.*, 2024) and with less extent to bypass transition (Duraisamy *et al.*, 2015) and natural transition (Yang & Xiao, 2020). However, the data-driven enhancement of separation induced transition flows using FIML has gained far less attention. Symbolic regression has been recently employed to train the laminar kinetic energy transition model, originally developed by Pacciani *et al.* (2011), to improve the predictions of bypass and separation in-

duced transition flows over low and high pressure turbine cascades (Akolekar *et al.*, 2021, 2022; Fang *et al.*, 2023). Nevertheless, data-driven modeling of separation induced transition for flows under moderate-to-high adverse pressure gradient for isolated airfoils still needs to be explored.

Here, we focus on the field inversion of the laminar kinetic energy model of Pacciani *et al.* (2011) and infer the corrections needed to its production term. In addition, we also use field inversion to directly infer the intermittency field of the shear stress transport $k-\omega$ turbulence model. Two cases are considered: The first is a flate plate with favorable and adverse pressure gradients; then we move forward with the static parametric series of NACA 0012 at chord-based Reynolds number, $Re = 200,000$ and angles of attack of 4°, 8°, 10°, and 12°. The dataset obtained from the field inversion should serve as a starting point for training a transition model, using machine learning algorithms to improve predictions of transitional flows with laminar separation bubbles.

FIELD INVERSION

Laminar Kinetic energy model

The baseline model used here is similar to the laminar kinetic energy transition model proposed by Pacciani *et al.* (2011). This model uses Wilcox's original $k-\omega$ model (Wilcox, 1988) as the underlying turbulence model, written in the incompressible form as follows.

$$\frac{Dk}{Dt} = \nabla\cdot\left[(\nu+\sigma_k\nu_t)\nabla k\right] - C_\mu k\omega + F_\mu P_k + R, \qquad (1)$$

$$P_k = min(\nu_t|S|^2, \frac{k|S|}{\sqrt{6}}), \qquad (2)$$

$$\frac{D\omega}{Dt} = \nabla\cdot\left[(\nu+\sigma_\omega\nu_t)\nabla\omega\right] - C_{\omega2}\omega^2 + C_{\omega1}F_\mu|S|^2, \qquad (3)$$

where $c_\mu = 0.09$, $c_{\omega1} = 5/9$, $c_{\omega2} = 3/40$ and $\sigma_k = \sigma_\omega = 0.5$. The eddy viscosity ν_t equals k/ω and $|S|$ is the strain rate magnitude given as $|S| = \sqrt{2S_{ij}S_{ji}}$. A limiter is used in the production of turbulent kinetic energy, P_k following Durbin & Reif (2010) to account for the stagnation-point anomaly which results in unphysical values of k near the stagnation point of an airfoil leading edge.

A function F_μ, which is defined in Pacciani *et al.* (2011), is used to damp the turbulence level prior to transition. The same damping function is used for both the production of k and of ω. It is noteworthy that the damping here is different from the original model, where the damping was applied to the eddy viscosity, instead of to the turbulent kinetic energy production term. Other damping functions were used for the production of ω and the dissipation of k. Here, we use only a single damping function for the k and ω production terms.

The transfer term R has opposite signs in turbulent and laminar kinetic energy equations, which implies energy transfer from laminar kinetic energy (k_ℓ) to turbulent kinetic energy (k). The laminar kinetic energy equation is given as

$$\frac{Dk_\ell}{Dt} = \nabla\cdot\nu\nabla k_\ell - 2\nu\frac{k_\ell}{y^2} + \beta P_\ell - R \qquad (4)$$

where $2\nu k_\ell/y^2$ is a dissipation term with y being the wall normal distance. The production term P_ℓ is given by

$$P_\ell = \nu_\ell|S|^2, \qquad (5)$$

$$\nu_\ell = C_1\sqrt{k_\ell}\delta_\Omega, \qquad (6)$$

$$\delta_\Omega = min(\frac{\Omega y^2}{U}, 2), \qquad (7)$$

where $C_1 = 0.006$ and ν_ℓ is the laminar eddy viscosity, expressed in terms of a velocity scale, $\sqrt{k_\ell}$ and a vorticity length scale, δ_Ω that depends on the vorticity magnitude, $\Omega = \sqrt{2\Omega_{ij}\Omega_{ji}}$, the wall distance, y and the velocity magnitude, U. The transfer term R is modeled similar to Pacciani *et al.* (2011)

The laminar kinetic energy production term in Eq. 4 is augmented with a corrective field, $\beta(\mathbf{x})$ which is obtained by solving the following optimization problem.

$$\beta = argmin\left[\sum_{wall}(\tau_w^{RANS}(\beta) - \tau_w^{data})^2 - \sum_{flow}\lambda(\beta-1)^2\right] \qquad (8)$$

The last term regularizes the optimization problem, with λ being a small number. The problem is to solve Eq. 8 with τ_w^{RANS} obtained by solving the RANS equations and τ_w^{data} being the data to fit.

Inference of Intermittency Field

In the second approach, we augment the production term of the turbulent kinetic energy of the $k-\omega$ SST model of Menter *et al.* (2003) with an intermittency field, γ_{eff}. The model is described as follows.

$$\frac{Dk}{Dt} = \nabla\cdot\left[(\nu+\sigma_k\nu_t)\nabla k\right] - C_\mu k\omega + \gamma_{eff}P_k, \qquad (9)$$

$$\frac{D\omega}{Dt} = \nabla\cdot\left[(\nu+\sigma_\omega\nu_t)\nabla\omega\right] - C_{\omega2}\omega^2 + \frac{C_{\omega1}}{\nu_t}P_k + 2(1-F_1)\frac{\sigma_{\omega2}}{\omega}\frac{\partial k}{\partial x_j}\frac{\partial\omega}{\partial x_j}. \qquad (10)$$

Here, the model coefficients are blended between inner and outer values, using the blending function, F_1. The details of the blending, the production term, P_k and the description of eddy viscosity, ν_t are provided by Menter *et al.* (2003).

Instead of inferring the intermittency (γ_{eff}) directly, it is described in terms of the discrepancy field β as follows.

$$\gamma_{eff} = (1-F_t)\beta + F_t, \qquad (11)$$

$$F_t = 0.5(1+tanh(10(\frac{k}{\omega\nu} - C_t))). \qquad (12)$$

This is to ensure that $\gamma = 1$ in the fully turbulent region. Prior to transition, the eddy viscosity ratio $k/(\omega\nu)$ is small and F_t is approximately zero. In the turbulent region, $k/(\omega\nu)$ increases until it exceeds a threshold value C_t (values of 10 and 20 are used) to force γ_{eff} to be equal to unity. This is considered to prevent the transition model interfering in the turbulent region.

Since the number of design variables involved in this optimization problem is large, we use gradient-based optimization with the discrete adjoint method. The open source module DAFoam has been used to solve the optimization problem, with OpenFoam for the CFD and Python's pyOptSparse module for the optimizer (Bidar *et al.*, 2022). DAFoam implements a discrete adjoint solver to compute gradients of the cost function with respect to the β field. The Python module performs a gradient-based optimization. The following sections show the implementation and the results for the flat plate with pressure gradient and the NACA 0012 parametric series.

FLAT PLATE WITH PRESSURE GRADIENTS

The computational domain for the flat plate case is shown in Fig. 1. The upper surface is a curved slip wall that provides favorable and adverse pressure gradients. The inlet is one half chord length upstream of the plate leading edge. The part of the bottom surface that extends from the inlet to the plate leading edge is specified as a symmetry plane, whereas the flat plate is defined as a no-slip surface. The number of cells is 149 in the stream-wise direction and 99 in the wall-normal direction.

Two test cases are considered at two different turbulent intensities. The LES data provided by Lardeau *et al.* (2012) are used as the high-fidelity data for inferring the corrections fields at turbulent intensity levels of 1.5% and 2% defined at the position corresponding to the mid-chord. The inlet conditions are given in Table 1; they were provided by Ge *et al.* (2014) to match the LES free-stream turbulent intensity level and dissipation rate. The regularization constant used for this case is $\lambda = 10^{-4}$ and the threshold value C_t used in Eq. 12 is 10.

Table 1. Inlet conditions for the flat plate case

	$U_{in}(m/s)$	$Tu_{in}\%$	$\omega_{in}(s^{-1})$	$\nu(m^2s^{-1})$
Case 1	0.9	5.8	90	1.5×10^{-5}
Case 2	0.9	7.5	60	1.5×10^{-5}

The skin friction distribution over the flat plate surface is shown in Figs. 2 & 3 for both the laminar kinetic energy (LKE) and SST-γ_{eff} models. The baseline LKE model shows earlier transition onset and slightly a delayed reattachment point, compared to LES data for case 1. The reattachment point is more delayed in case 2. It was recommended by Pacciani *et al.* (2014) that the production term of the LKE model should depend on the free-stream turbulent intensity, which was not used here. This is the reason why the baseline LKE model results are similar for cases 1 and 2, while the LES data exhibits different reattachment points. However, free-stream intensity is accounted for through field inversion, which shows that the optimized LKE model (LKE-FI) fits well with the data up to the reattachment point. Beyond this, discrepancies start to emerge, which shows that the field inversion has limited impact on the fully turbulent flow beyond the reattachment point. This limited impact is more clear in case 2.

Similarly, the corrected SST model ($k-\omega$ SST-FI) fits well with the data up to the reattachment point. The blending function shown in Eq. 12 limits model corrections in the turbulent flow beyond the reattachment point. Figs. 4 & 5 show the contours of β for case 1. In both models, β is decreased in the laminar region and then increases towards transition to force the flow to reattach on time. It is noticed in Fig. 5 that β increases near the wall beyond the reattachment point. This is because the eddy viscosity ratio is small near the wall, leading to F_t being almost zero, which can result in changes of γ_{eff}. However, this seems to have limited impact on the turbulent region, as shown from the skin friction coefficient behavior in Figs. 2 and 3.

NACA 0012 PARAMETRIC SERIES

The O-grid topology used for the airfoil case is shown in Fig. 6. The domain radius is 20 times the chord length, and the number of cells is 887 along the airfoil surface and 179 in the wall normal direction. The first cell height is chosen such that $y_+ <= 1$ everywhere on the airfoil surface. The inlet turbulent intensity is 1% with an eddy viscosity ratio of unity. The field inversion is carried out at a chord Reynolds number of 200,000 and four angles of attack $\alpha = 4^\circ$, 8°, 10°, and 12°. The regularization constant is 10^{-4} for $\alpha = 4^\circ$ and 10^{-6} for higher angles of attack.

To supply high-fidelity data for field inversion, well-resolved LES data have been generated for a NACA 0012 airfoil at the aforementioned angles of attack. The LES code utilizes high-order schemes for solving finite difference formulations of the Navier-Stokes equations, with time integration by an implicit Beam-Warming scheme; see Sharma & Visbal (2019) for further discussion of the solver. Once the simulation reached statistically steady conditions, the data were time-averaged and subsequently span-averaged.

The skin friction distribution over the airfoil upper surface is shown in Figs. 7-10. For the case $\alpha = 4^\circ$, The LES data exhibit a small separation bubble, centered at $x/c \approx 0.42$, which the baseline LKE model fails to predict because the transition is too early. The optimized model accounts for this by reducing the production term, to delay transition. Both LKE-FI and $k-\omega$ SST-FI models fit the data well up to the end of transition. It can be seen that the optimized models do not fit the data in the turbulent region beyond flow transition. In $k-\omega$ SST-FI model, optimization is stopped in this region due to the threshold value for blending, $C_t = 20$.

For higher angles of attack, the LKE model exhibited very quick transition near the leading edge. The correction for this behavior resulted in numerical instability and oscillatory c_f distribution. Hence, only the results for $k-\omega$ SST are reported for angles of attack 8°, 10°, and 12° in Figs. 8-10. The c_f distribution shows that the laminar separation bubble becomes smaller and moves towards the airfoil leading edge as the angle of attack increases. The corrected $k-\omega$ SST model fits well with the LES data for all cases. In the case $\alpha = 4^\circ$, the variations in β span the airfoil upper surface, as shown in Fig. 11, since the separation bubble is close to the airfoil mid-chord. At higher angles of attack, the model corrections are near the leading edge (Figs. 12 & 13). It should be noted that γ_{eff} was inferred directly without the blending used in Eq. 11 for higher angles of attack, as the discrepancies were mainly in the separation bubble near the leading edge.

CONCLUSION

Field inversion of two RANS models were carried out to enhance their predictions for separation-induced transition flows. The first model is a laminar kinetic energy model, originally capable of predicting transition, whereas the second model is the $k-\omega$ SST turbulence model supplemented by an intermittency function. The cases considered are a flat plate below a curved upper surface that provides favorable and adverse pressure gradients, and an NACA 0012 parametric series, which exhibits separation-induced transition, with laminar separation bubbles. While the field inversion of $k-\omega$ SST was successful for all the cases presented, the LKE model was limited to the flat plate case and NACA 0012 at $\alpha = 4^{\circ}$. The present data set is a starting point for training a data-driven model to characterize separation-induced transition, which plays a significant role in dynamic stall onset over pitching airfoils.

REFERENCES

Akolekar, Harshal D, Pacciani, Roberto, Waschkowski, Fabian & Zhao, Yaomin 2022 Multi-Objective Development Of Machine-Learnt Closures For Fully Integrated Transition And Wake Mixing Predictions In Low Pressure Turbines. In *Proceedings of the ASME Turbo Expo*, , vol. 10-C.

Akolekar, Harshal D., Waschkowski, Fabian, Zhao, Yaomin, Pacciani, Roberto & Sandberg, Richard D. 2021 Transition modeling for low pressure turbines using computational fluid dynamics driven machine learning. *Energies* **14** (15).

Bidar, Omid, He, Ping, Anderson, Sean & Qin, Ning 2022 An Open-source Adjoint-based Field Inversion Tool for Data-driven RANS Modelling. *AIAA AVIATION 2022 Forum* pp. 1–14.

Duraisamy, Karthik, Singh, Anand Pratap & Pan, Shaowu 2017 Augmentation of turbulence models using field inversion and machine learning. In *AIAA SciTech Forum - 55th AIAA Aerospace Sciences Meeting*. American Institute of Aeronautics and Astronautics Inc.

Duraisamy, Karthik, Zhang, Ze Jia & Singh, Anand Pratap 2015 New approaches in turbulence and transition modeling using data-driven techniques. In *53rd AIAA Aerospace Sciences Meeting*. American Institute of Aeronautics and Astronautics Inc, AIAA.

Durbin, P. A. & Reif, B. A. Pettersson 2010 *Statistical Theory and Modeling for Turbulent Flows*. Wiley.

Fang, Yuan, Zhao, Yaomin, Akolekar, Harshal D, Ooi, Andrew S.H., Sandberg, Richard D, Pacciani, Roberto & Marconcini, Michele 2023 A Data-Driven Approach for Generalizing The Laminar Kinetic Energy Model for Separation and Bypass Transition in Low- and High-Pressure Turbines. In *Proceedings of the ASME Turbo Expo*, , vol. 13C.

Garmann, Daniel J. & Visbal, Miguel R. 2011 Numerical investigation of transitional flow over a rapidly pitching plate. *Physics of Fluids* **23** (9).

Ge, Xuan, Arolla, Sunil & Durbin, Paul 2014 A bypass transition model based on the intermittency function. *Flow, Turbulence and Combustion* **93** (1), 37–61.

Lardeau, Sylvain, Leschziner, Michael & Zaki, Tamer 2012 Large Eddy Simulation of transitional separated flow over a flat plate and a compressor blade. *Flow, Turbulence and Combustion* **88** (1-2), 19–44.

Ling, Julia, Jones, Reese & Templeton, Jeremy 2016 Machine learning strategies for systems with invariance properties. *Journal of Computational Physics* **318**, 22–35.

Menter, F R, Kuntz, M & Langtry, R 2003 Ten Years of Industrial Experience with the SST Turbulence Model Turbulence heat and mass transfer. *Turbulence, Heat and Mass Transfer* **4** (July 2014), 625–632.

Oliver, Todd A & Moser, Robert D 2011 Bayesian uncertainty quantification applied to RANS turbulence models. In *Journal of Physics: Conference Series*, , vol. 318, p. 042032.

Pacciani, Roberto, Marconcini, Michele, Arnone, Andrea & Bertini, Francesco 2014 Predicting High-Lift Low-Pressure Turbine Cascades Flow Using Transition-Sensitive Turbulence Closures. *Journal of Turbomachinery* **136** (5).

Pacciani, Roberto, Marconcini, Michele, Fadai-Ghotbi, Atabak, Lardeau, Sylvain & Leschziner, Michael A. 2011 Calculation of high-lift cascades in low pressure turbine conditions using a three-equation model. *Journal of Turbomachinery* **133** (3).

Parish, Eric J. & Duraisamy, Karthik 2016 A paradigm for data-driven predictive modeling using field inversion and machine learning. *Journal of Computational Physics* **305**, 758–774.

Rumsey, C. L., Coleman, G. N. & Wang, L. 2022 In Search of Data-Driven Improvements to RANS Models Applied to Separated Flows. In *AIAA Science and Technology Forum and Exposition, AIAA SciTech Forum 2022*. American Institute of Aeronautics and Astronautics Inc, AIAA.

Sharma, Anupam & Visbal, Miguel 2019 Numerical investigation of the effect of airfoil thickness on onset of dynamic stall. *Journal of Fluid Mechanics* **870**, 870–900.

Singh, Anand Pratap, Matai, Racheet, Duraisamy, Karthik & Durbin, Paul 2017 Data-driven augmentation of turbulence models for adverse pressure gradient flows. In *23rd AIAA Computational Fluid Dynamics Conference, 2017*. American Institute of Aeronautics and Astronautics Inc, AIAA.

Srivastava, Vishal, Rumsey, Christopher L., Coleman, Gary N. & Wang, Li 2024 On Generalizably Improving RANS Predictions of Flow Separation and Reattachment. American Institute of Aeronautics and Astronautics (AIAA).

Tracey, Brendan, Duraisamy, Karthik & Alonso, Juan J. 2013 Application of supervised learning to quantify uncertainties in turbulence and combustion modeling. In *51st AIAA Aerospace Sciences Meeting including the New Horizons Forum and Aerospace Exposition 2013*. American Institute of Aeronautics and Astronautics Inc.

Visbal, Miguel R. 1990 Dynamic stall of a constant-rate pitching airfoil. *Journal of Aircraft* **27** (5), 400–407.

Visbal, Miguel R. & Garmann, Daniel J. 2018 Analysis of dynamic stall on a pitching airfoil using high-fidelity large-eddy simulations. In *AIAA Journal*, , vol. 56, pp. 46–63.

Wang, Jian Xun, Wu, Jin Long & Xiao, Heng 2017 Physics-informed machine learning approach for reconstructing Reynolds stress modeling discrepancies based on DNS data. *Physical Review Fluids* **2** (3), 034603.

Weatheritt, Jack & Sandberg, Richard 2016 A novel evolutionary algorithm applied to algebraic modifications of the RANS stress–strain relationship. *Journal of Computational Physics* **325**, 22–37.

Wilcox, David C. 1988 Reassessment of the scale-determining equation for advanced turbulence models. *AIAA Journal* **26** (11), 1299–1310.

Wu, Jin Long, Xiao, Heng & Paterson, Eric 2018 Physics-informed machine learning approach for augmenting turbulence models: A comprehensive framework. *Physical Review Fluids* **7** (3), 074602.

Yang, Muchen & Xiao, Zhixiang 2020 Improving the k- ω- γ- Artransition model by the field inversion and machine learning framework. *Physics of Fluids* **32** (6).

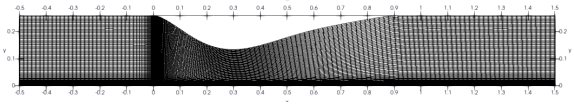

Figure 1. The computational mesh for the flat plate case

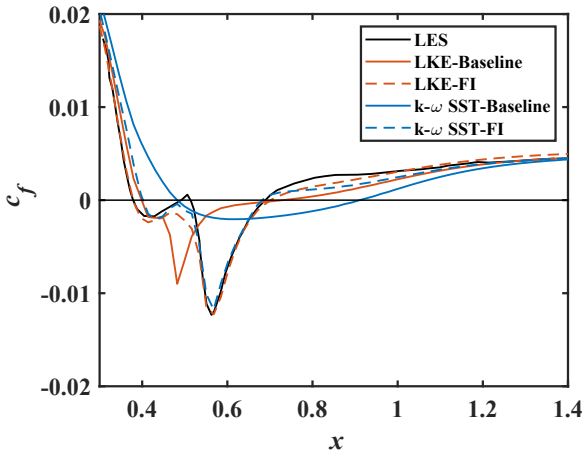

Figure 2. Skin friction coefficient distribution for the flat plate case 1.

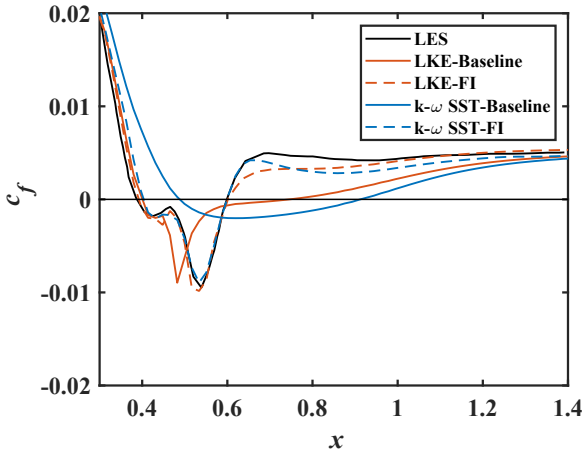

Figure 3. Skin friction coefficient distribution for the flat plate case 2.

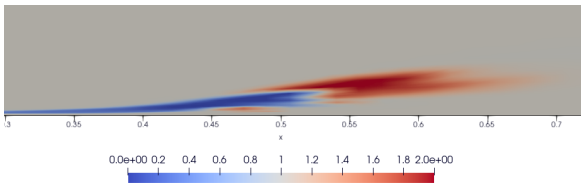

Figure 4. Inferred β field for the flat plate case 1 using the LKE model.

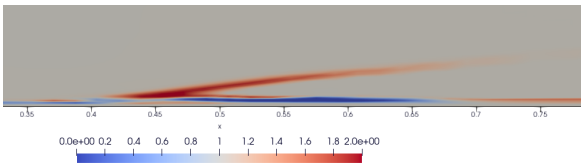

Figure 5. Inferred β field for the flat plate case 1 using $k-\omega$ SST model.

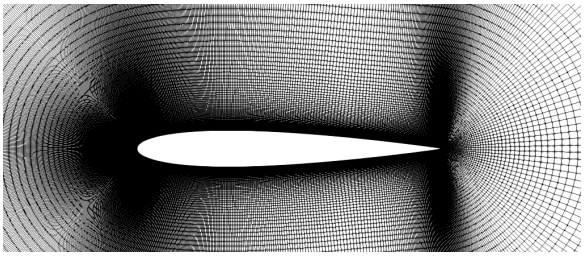

Figure 6. The computational mesh for the airfoil case

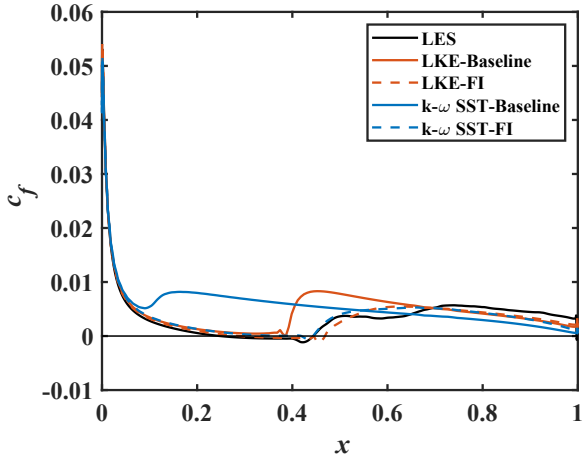

Figure 7. Skin friction coefficient distribution for NACA 0012 at $\alpha = 4°$.

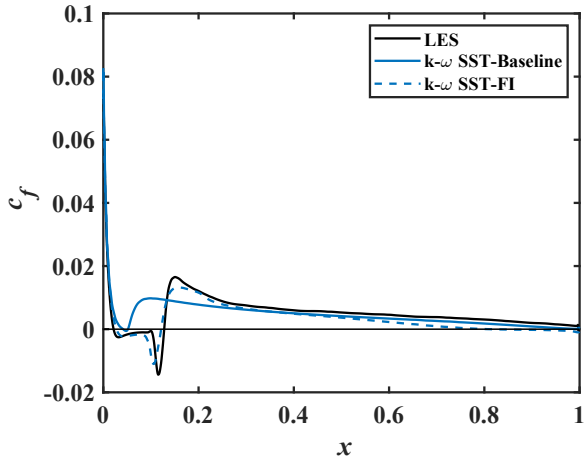

Figure 8. Skin friction coefficient distribution for NACA 0012 at $\alpha = 8°$.

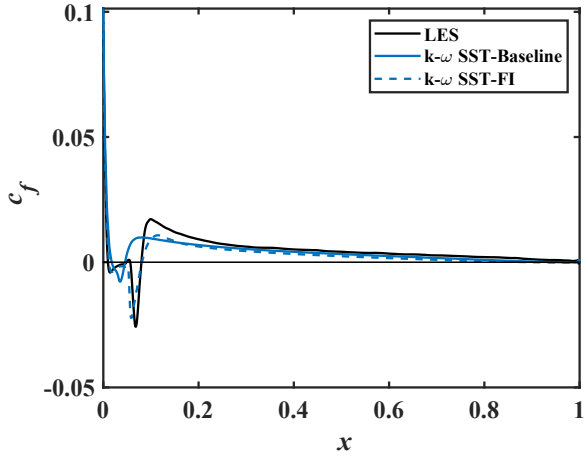

Figure 9. Skin friction coefficient distribution for NACA 0012 at $\alpha = 10°$.

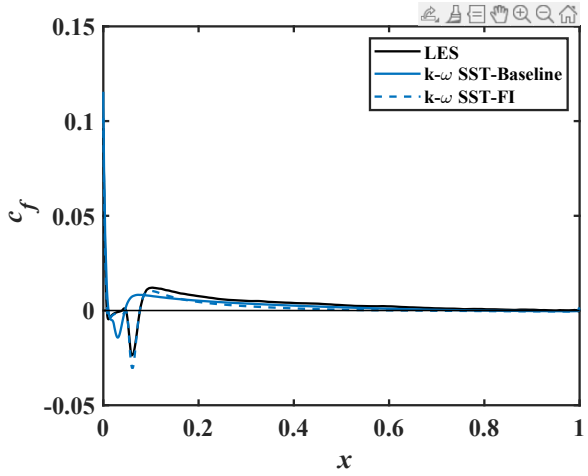

Figure 10. Skin friction coefficient distribution for NACA 0012 at $\alpha = 12°$.

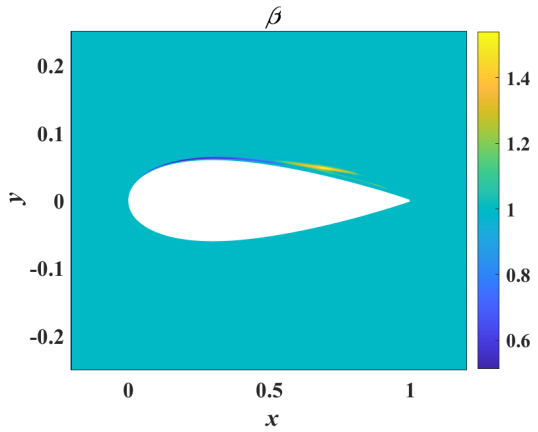

Figure 11. Inferred β field for NACA 0012 at $\alpha = 4°$ using $k-\omega$ SST model.

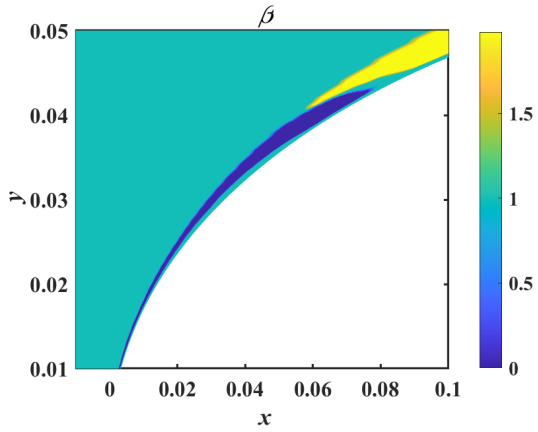

Figure 12. Inferred β field for NACA 0012 at $\alpha = 10°$ using $k-\omega$ SST model.

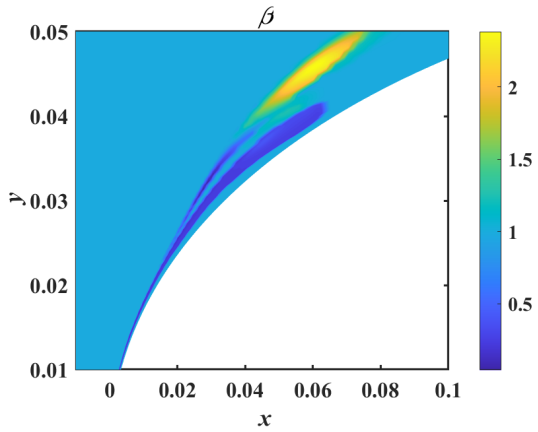

Figure 13. Inferred β field for NACA 0012 at $\alpha = 12°$ using $k-\omega$ SST model.